Title

Image-Guided Ablation of Dental Calculus From Root Surfaces Using a DPSS Er:YAG Laser

Journal

Lasers in Surgery and Medicine, 52(3)

ISSN

1050-9267

Authors

Fried, William A
Chan, Kenneth H
Darling, Cynthia L
et al.

Publication Date

2020-03-01

DOI

10.1002/lsm.23122

Peer reviewed

HHS Public Access

Author manuscript

Lasers Surg Med. Author manuscript; available in PMC 2022 February 25.

Published in final edited form as:

Lasers Surg Med. 2020 March ; 52(3): 247–258. doi:10.1002/lsm.23122.

Image-Guided Ablation of Dental Calculus From Root Surfaces Using a DPSS Er:YAG Laser

William A. Fried, BSc, **Kenneth H. Chan, PhD**, **Cynthia L. Darling, PhD**, **Donald A. Curtis, DDS**, **Daniel Fried, MS, PhD***

University of California, San Francisco, San Francisco, California, 94143

Abstract

Background and Objectives: Recent studies have demonstrated that near-infrared (IR) imaging can be used to acquire high-contrast images of root caries and calculus on the root surfaces of extracted teeth at wavelengths longer than 1450 nm. The purpose of this study was to determine if image-guided laser ablation can be used to selectively remove calculus from tooth surfaces with minimal damage to the underlying sound cementum and dentin.

Materials and Methods: In this study, sequential near-IR images at 1500–1700 nm were used to guide a diode-pumped (DPSS) Er:YAG laser for the removal of calculus from the root surfaces of 10 extracted teeth. The selectivity of removal was assessed using digital microscopy, optical coherence tomography, and surface profilometry.

Results: Calculus was removed rapidly with minimal damage to the underlying sound cementum and dentin. Image-guided ablation achieved high-selectivity, the mean volume of calculus removal was more than 27 times higher than the mean loss of cementum.

Conclusions: We have demonstrated that near-IR image-guided laser ablation can be used for the selective removal of calculus from root surfaces *ex vivo*. Additionally, we have demonstrated that a diode-pumped solid-state Er:YAG laser is well suited for selective removal.

Keywords

dental calculus; selective laser ablation; image-guided ablation

INTRODUCTION

Calculus can form sub- and supragingivally and can contribute to irritation and inflammation of the gingiva that may lead to gingivitis and periodontitis. Scaling and root planing are often recommended to remove the calculus. Improved visualization of that calculus is important for both monitoring and complete removal. Several approaches have been used to image calculus including fluorescence-based methods [1–10], Raman spectroscopy [11–

*Correspondence to: Daniel Fried, MS, PhD, Department of Preventive and Restorative Dental Sciences, Division of Biomaterials and Bioengineering, University of California, San Francisco, 707 Parnassus Avenue, San Francisco, CA 94143-0758. Daniel.fried@ucsf.edu.

Conflict of Interest Disclosures: All authors have completed and submitted the ICMJE Form for Disclosure of Potential Conflicts of Interest and none were reported.

13] and optical coherence tomography (OCT) [11,14–16]. Near-infrared (NIR) reflectance imaging at longer wavelengths is also advantageous for imaging dental calculus or mineralized dental plaque on tooth surfaces due to the lack of interference of stains and the higher light scattering of mineralized plaque [16].

Multiple *in vitro* and *in vivo* studies evaluating the coronal surfaces of teeth have demonstrated that NIR reflectance imaging yields higher contrast between demineralized and sound tooth structure than visible reflectance and fluorescence. Much of this difference is due to the lack of interference from stains, stains do not interfere at wavelengths longer than 1200 nm [17–22]. Visible and fluorescence-based caries detection systems suffer from false positives resulting from stains [23–28]. Studies show that stains completely mask demineralization on tooth occlusal surfaces [20,29]. Highly conjugated molecules such as melanin and porphyrins produced by bacteria as well as those found in food dyes accumulate in dental plaque. They are responsible for the pigmentation in the visible range and do not absorb light beyond 1200 nm [30–32]. Imaging root caries at longer NIR wavelengths appears to be equally advantageous due to the lack of interference of stains beyond 1200 nm. Root caries are often heavily stained and it can be difficult to differentiate between stained eroded areas (affected dentin) and root caries (demineralized dentin/cementum). In addition, there is increased suppression of the reflectivity from the sound dentin due to the higher water absorption that increases markedly beyond 1400 nm [16]. The amount of reflected light (backscattered) from the underlying dentin depends on the ratio of scattering to absorption. Therefore, wavelengths with higher water absorption can yield high lesion contrast even though the light scattering in sound dentin is still relatively high.

Several studies have been carried out using lasers for the removal of calculus including the Er:YAG laser [33–38]. DPSS Er:YAG lasers with high pulse repetition rates are more suitable for the selective removal of dental caries, composites, and calculus than existing Er:YAG lasers [39]. The flash-lamp pumped erbium solid-state lasers presently being used for dental hard tissue ablation are poorly suited for this approach since they utilize high energy pulses and relatively low pulse repetition rates. DPSS Er:YAG lasers are now available operating with pulse repetition rates as high as 1–2 kHz and initial studies have been carried out demonstrating their utility for the ablation of dental hard tissues and bone [40–42] and the removal of composite from tooth surfaces [43].

Demineralized dental hard tissues are typically removed at higher rates than sound tissues due to the higher ratio of water, protein, and lipid to mineral, offering some level of selectivity without additional feedback. In the visible range stains in caries lesions also have increased absorption. Several studies report the selective removal of caries lesions using various lasers including the Nd:YAG [44,45], Er:YAG [46], frequency doubled alexandrite (377 nm), frequency-tripled Nd:YAG (355 nm), [47–51] and excimer [52]. The same principle can be applied for the removal of calculus from tooth surfaces using ultraviolet and visible laser pulses [36,53,54].

Previous approaches for guiding laser ablation on tooth surfaces have included fluorescence [55–57] and NIR transillumination [58]. In addition to investigating the selective removal

of caries lesions with a fluorescence-based feedback system, Krause et al. [59] investigated the removal of calculus. Image-guided laser ablation requires the rapid acquisition of high-contrast images of caries lesions or calculus that can be coupled to the laser-scanning system for selective removal. Computer control is now feasible due to the recent advances in compact high-speed laser-scanning technology such as micro-electro-mechanical systems mirrors and miniature galvanometer “galvo” based scanners. One approach is to remove the lesion or calculus layer by layer, that is, image the lesion then scan the laser and remove an outer layer of the lesion, then re-image and scan again repeating that process until the lesion is completely removed. Previous studies have demonstrated the feasibility of removing caries lesions by sequentially imaging carious teeth with an NIR InGaAs camera or coaxial NIR laser as the CO_2 laser removes the lesion layer by layer [60–62]. Spectral feedback has also been employed successfully with lasers to remove composite from tooth surfaces [43,63–65]

The purpose of this study was to explore the potential of using near-IR reflectance imaging with a DPSS Er:YAG laser for the image-guided ablation of dental calculus from root surfaces.

MATERIALS AND METHODS

Sample Preparation

Thirty extracted teeth from patients in the San Francisco Bay Area were collected, cleaned, and sterilized with Gamma radiation and stored in a 0.1% thymol solution. From the 30 extracted teeth, 10 samples with prominent calculus deposits were selected. Calculus was easily identified as dark gray or black clumps stuck to the tooth surface below the cementum enamel junction (CEJ). Since calculus deposits protrude above the tooth cementum, calculus presence was confirmed using OCT. Teeth were mounted on 1 × 1 × 3 cm cylindrical blocks of black orthodontic composite resin with the root surface containing the lesions facing out from the square surface of the block. Each rectangular block fit precisely in an optomechanical assembly that could be positioned with micron accuracy. The samples were stored in a moist environment and they were air-dried with compressed air for 10 seconds before measurement.

Visible and NIR Cross Polarization Reflectance Images (NIR)

Visible color images of the samples were acquired using a USB microscope, Model AM7915MZT from AnMO Electronics Corp. (New Taipei City, Taiwan) with extended depth of field and cross polarization. The digital microscope captures 5 megapixels (2,952 × 1,944) color images.

In order to acquire reflected light images, linearly polarized and collimated light from a 150-W fiber-optic illuminator, Model FOI-150 from the E. Light Company (Denver, CO) was used to illuminate the samples at an incident angle of 30°. Polarizers were placed after the light source and before the detector to remove specular reflection (glare) that interferes with measurements of the lesion contrast. The NIR reflectance images were captured using a 12-bit Model GA1280J (Sensors Unlimited, Princeton, NK) with a 1,280 × 1,024 pixel

format and 15-μm pixel pitch using a Model SWIR-35 lens from Navitar, Inc. (Rochester, NY). Reflectance measurements were taken with a 1500-nm long-pass filter, the FEL 1500 from Thorlabs (Newton, NJ).

Laser Setup and Parameters

Samples were irradiated using a DPSS Er:YAG laser, Model DPM-30 from Pantec Engineering (Liechtenstein) operated with a pulse duration of 50-μs and a pulse repetition rate of 50-Hz (Fig. 1). The laser energy output was monitored using a power meter EPM 1000, Coherent-Molectron (Santa Clara, CA), and the Joulemeter ED-200 from Gentec (Quebec, Canada). A high-speed XY-scanning system, Model ESP 301 controller with ILS100PP and VP-25AA stages from Newport (Irvine, CA) was used to scan the samples across the laser beam. Designated areas on each tooth were irradiated by the laser using the computer controlled XY-scanning system. The laser was focused to a spot size of ~330 μm using a ZnSe lens of 75 mm focal length. A pressure air-actuated fluid spray delivery system consisting of a 780S spray valve, a Valvemate 7040 controller, and a fluid reservoir from EFD, Inc. (East Providence, RI) were used to provide a uniform spray of fine water mist onto the tooth surfaces at 2 ml/min. An incident fluence of 9 J/cm^2 was used to remove the calculus from tooth surfaces.

Digital Microscopy

Tooth surfaces were examined after laser irradiation using an optical microscopy/3D surface profilometry system, the VHX-1000 from Keyence (Elmwood, NJ). Two lenses were used, the VH-Z25 with magnification from ×25 to 175 and the VH-Z100R with a magnification of ×100–1000. Depth composition digital microscopy images and three-dimensional (3D) images were acquired by scanning the image plane of the microscope and reconstructing a depth composition image with all points at optimum focus displayed in a 2D image. The Keyence 3D measurement software, VHX-H3M, was used to examine the laser-irradiated surfaces for residual calculus and damage to the underlying cementum.

Imaging, Processing, and Calculus Removal

Samples were air-dried for ~10 seconds prior to acquisition of NIR images of the root surface of each tooth. To obtain accurate backscattered light intensity values in NIR reflectance images from a non-uniform illumination source, NIR reflectance images were calibrated with a background reference. Prior to image acquisition, NIR reflectance images of barium sulfate were taken to produce a suitable reference to define the diffusive light distribution emanating from the light source. The reference image A was normalized under its maximum value to a double float precision decimal between 0 and 1. Then the original image B was divided by the normalized reference image A′ to represent an amended NIR reflectance image B′.

$$A' = A/A_{MAX}$$

$$B' = B/A'$$

In the next step, the contrast map was constructed using the amended image mentioned above. The determination of the contrast was calculated through a semiautomatic process. Intensity values from the initial scan were collected and reused throughout the caries removal process to maintain repeatability in lesion segmentation. The mean intensity of the root surface I_R was calculated over a region of exposed sound root surface and the maximum intensity of the calculus I_C was collected inside the area with calculus. The pixel contrast C was computed by subtracting the intensity of the image pixel I_P with the mean intensity of root surface and the minimum value I_{MIN} in each image and dividing this difference over the maximum intensity. An image ablation map or look-up table (LUT) was generated by comparing the pixel contrast to a specified threshold over the enhanced NIR image.

If $C = (I_P - I_{MIN} - I_R)/I_C > T$; add pixel to LUT

Samples were mounted on a separate system for Er:YAG laser ablation, and positioned precisely to match the same orientation used for NIR imaging. Repeated serial NIR images and LUT were taken and generated with the same threshold value and teeth were ablated until the calculus was removed. All image analysis was carried out using Labview from National Instruments (Austin, TX) and IGOR Pro software (Wavemetrics, Lake Oswego, OR).

Optical Coherence Tomography

A single-mode fiber, autocorrelator-based Optical Coherence Domain Reflectometry (OCDR) system with an integrated fiber probe, high-efficiency piezoelectric fiber-stretchers and two balanced InGaAs receivers that was designed and fabricated by Optiphase, Inc. (Van Nuys, CA) was integrated with a broadband high power superluminescent diode (SLD), DL-CS313159A from Denselight (Jessup, MD) operating at 1304 nm with an output power of 19 mW and a bandwidth of 83 nm and a high-speed XY-scanning system, ESP 300 controller & 850-HS stages from Newport (Irvine, CA) and used for *in vitro* optical tomography. The fiber probe was configured to provide an axial resolution at 9-μm in air and a lateral resolution of approximately 50-μm over the depth of focus of 10-mm.

The all-fiber OCDR system has been previously described in greater detail [66]. The OCT system is completely controlled using Labview™ software from National Instruments (Austin, TX). Acquired scans are compiled into *b-scan* files. Image processing was carried out using Igor Pro™, data analysis software from Wavemetrics Inc, (Lake Oswego, OR). The processed images were then analyzed using Avizo 3D data visualization software from ThermoFisher (Hillsboro, OR).

RESULTS

Color images acquired before and after calculus removal are shown in Figure 2 for four of the teeth. Most of the calculus was removed in the area scanned by the laser. After removal of the calculus many of the teeth have residual stained areas visible at the periphery of

the laser-irradiated zone. Most likely, these deposits are either non-calcified plaque or some other organic material that has attached itself to the tooth surface. Sample B is a good example of residual staining showing a continuous brown ring around the laser-irradiated area. Only calcified plaque and areas of demineralization are visible in the NIR, and stained areas and non-calcified plaque are not identified for laser removal. In addition, there are some small residual calculus deposits visible. These deposits appear whiter than the surrounding tooth structure which suggests they are residual calculus. In addition, OCT scans indicate that they protrude above the root surface. It is possible that these isolated residual deposits of calculus have been modified by repeated scans from the laser, rendering them with higher mineral content and more resistant to further removal.

The maximum initial calculus thickness, the maximum height of residual calculus left on the surface, and the maximum depth of cementum removal are tabulated in Table 1 for each of the 10 samples. The initial calculus thickness varied from 0.33 to 0.92 mm on the root surface. The cementum loss was also measured at two different distances from the CEJ, within 1.5 mm and at distances greater than 1.5 mm to determine if the loss was likely due to root caries lesions. Root caries are typically located within 1.5 mm of the CEJ and a higher level of cementum and dentin loss near the CEJ would suggest that underlying root caries is the cause. Demineralized areas appear similar to calculus in near-IR images and so it is not surprising that both would be removed by the laser. Cementum damage was higher near the CEJ than further away from the CEJ (0.19 ± 0.095 vs. 0.15 ± 0.11) but the difference was not statistically significant ($P > 0.05$). There was a significant correlation between the initial calculus thickness and the residual calculus thickness $R^2 = 0.41$ but there was no significant correlation between the initial calculus thickness and the cementum loss.

Figures 3 and 4 show color images before and after calculus removal and sequential near-IR images taken during the removal process. In the near-IR, the highly reflective calculus deposits were completely removed at the end of the sequence of scans. There are some weakly reflective areas in the final near-IR images and those locations match the whiter areas in the color images after removal. For example, the whiter areas near the apex of the tooth root in Figure 4E match the whiter areas in Figure 4C*.

Figures 5 and 6 show a composite of color, near-IR, OCT, and high-resolution digital microscopy images of two samples before and after calculus removal. There is little damage to the underlying cementum for the tooth shown in Figure 5. The OCT scan shows that the tooth surface is intact and the thick layer of cementum was removed. Close examination of the high-resolution digital microscopy image (M2) shows a slight grid pattern in the tooth surface caused by the laser-scanning pattern. However, that damage is insufficient to be visible on the OCT scans and is likely superficial. For the tooth shown in Figure 6, there is damage to the underlying cementum. The cementum damage appears localized to a pit and is deep which suggests that it may be due to localized demineralization under the cementum. In the high-resolution digital microscopy image (M2) a pattern in the root surface due to the laser-scanning pattern is also visible.

The volume of calculus removed and the volume of the underlying cementum and dentin that was lost was determined using Avizo, a 3D data visualization program. These

calculations required individual analysis of a large number of parallel OCT b-scans. Two approaches were applied; in the first approach that was applied to 3 samples, every b-scan was analyzed. In the second approach completed on all 10 samples, five evenly spaced slices were measured for a partial volume analysis and the data were used to determine the ratio of cementum lost to calculus removed.

Figure 7 shows 3D surface renderings of the volumes of calculus (purple) and cementum lost (green) for the three teeth that underwent complete volumetric analysis using Avizo. Examination of the cementum loss indicates that it is distributed widely over the area underlying the calculus and is not localized to the margins of the calculus deposits. The largest area of cementum loss occurred on the second tooth, Figure 7B. Most of the cementum lost is within 1–2 mm of the CEJ. The volume of cementum lost for that tooth was 0.209 mm^3. This tooth suffered the greatest loss of cementum of all the samples. The area irradiated on the root surface was fairly large ~15mm^2 which means that the mean depth lost under the area of cementum removed was 140 μm for that tooth if the loss was evenly distributed over the surface. The volume of cementum removed does account for cementum being intact or demineralized prior to calculus removal. It is difficult to know for certain without sectioning if there was existing demineralization under the calculus deposits prior to removal.

The ratio of the amount of calculus removed to the cementum lost for all 10 samples was calculated by completing five evenly spaced OCT slices on each tooth in Avizo. The average amount of calculus removed was more than 27 times the amount of cementum removed.

DISCUSSION

An incident fluence of 9 J/cm^2 was sufficient to remove almost all the calculus within the treatment area. However, most of the samples had a few small residual calculus deposits and one sample had a significant amount of residual calculus remaining after many repeated scans. We can speculate that these residual deposits of calculus have been modified by laser irradiation after repeated scans from the laser, making them more resistant to further attempts to remove them. Preferential removal of water and organic components of the calculus may increase the fraction of mineral leaving highly mineralized deposits that are more difficult to remove. Stains that were not detectable within the NIR and not targeted by the laser also remained on the tooth after treatment. Most likely, these stains are either non-calcified plaque or some other organic material that has attached itself to the tooth surface.

The ratio of calculus to cementum removed was extremely high, more than 27 times higher. However, in some areas, the cementum loss was localized and as deep as 400 μm. This suggests that there may have been some areas of demineralization under the calculus due to the presence of root caries. Strong scattering by the overlying calculus prevented the identification of any demineralization under the calculus during the initial OCT scans. Root caries are typically located within 1.5 mm of the CEJ and a higher level of damage close to the CEJ would suggest that underlying root caries was the cause. When evaluating all 10 teeth, there was a higher level of cementum loss near the CEJ but the difference was

not statistically significant. Cementum loss may also occur due to alignment errors between the images and the laser-scanning system. Alignment of the laser to the start position of each scan is done manually, and positioning errors could result in inadvertent cementum ablation. However, this error should be more evident near the laser scan boundaries, yet the cementum loss was not localized to the periphery of the scan region. It was observed that often very large fragments of calculus fractured off from the tooth surface during removal. Some of the underlying cementum may have also fractured off from the tooth during the ejection of large calculus fragments. In addition, any cementum freshly exposed in the area under the ejected calculus fragment would be irradiated by the laser during the same scan thus removing cementum from that area. Exposed root surfaces also suffer from considerable erosion and it is possible that some of the cementum under the calculus was damaged or eroded prior to removal. Most likely a mix of alignment errors, fragmentation of the calculus, and the presence of root caries that has compromised the cementum layer underneath the calculus are responsible for damage to the cementum. Deeper lesions close to the CEJ are most likely the result of root caries while shallower grooves further from the CEJ are probably due to other sources. For clinical use, the handpiece will need to be fixed in place to avoid movement. In a previous clinical study, we constructed a spectral-guided laser ablation system and used bite blocks to fix the laser scanning in place [65]. We have also demonstrated that alignment errors can be greatly reduced by using coaxial ablation and imaging lasers so that the imaging and ablation can be done without changing position [61]. This approach removes any alignment errors and is less expensive since an InGaAs camera is not needed for the system.

The DPSS Er:YAG laser is capable of operating at pulse repetition rates of 1–2 kHz, a factor of 20–40 higher than the 50 Hz rate employed in this study. Future studies will employ higher pulse repetition rates for faster removal times. Peripheral thermal damage due to heat accumulation will also need to be explored at higher pulse repetition rates.

The proposed technique is a proof-of-concept study showing laser removal of calculus while limiting damage to cementum or dentin. Conventional approaches using power-driven and hand instruments including ultrasonic methods result in significant loss of cementum [67] and repeated and frequent root planing can result in the complete loss of cementum and erosion of the underlying dentin. Therefore, any methods that can potentially reduce the loss of cementum is a significant step forward. The technique would also be helpful in identifying a baseline of calculus present, and verification that calculus has been removed. The authors see the potential for improved visual feedback to patients, having a baseline comparison of calculus deposits over successive recall appointments.

CONCLUSION

We have demonstrated that near-IR image-guided laser ablation can be used for the selective removal of calculus from root surfaces. Additionally, we have demonstrated that a DPSS Er:YAG laser is well suited for selective removal.

ACKNOWLEDGEMENT

This work was supported by NIH/NIDCR Grant R01-DE19631.

Contract grant sponsor: NIH/NIDCR; Contract grant number: R01-DE19631.

REFERENCES

1. Badran Z, Demoersman J, Struillou X, Boutigny H, Weiss P, Soueidan A. Laser-induced fluorescence for subgingival calculus detection: Scientific rational and clinical application in periodontology. Photomed Laser Surg 2011;29(9):593–596. [PubMed: 21495861]
2. Folwaczny M, Heym R, Mehl A, Hickel R. Subgingival calculus detection with fluorescence induced by 655 nm InGaAsP diode laser radiation. J Periodontol 2002;73(6):597–601. [PubMed: 12083531]
3. Folwaczny M, Heym R, Mehl A, Hickel R. The effectiveness of InGaAsP diode laser radiation to detect subgingival calculus as compared to an explorer. J Periodontol 2004;75(5):744–749. [PubMed: 15212357]
4. Krause F, Braun A, Frentzen M. The possibility of detecting subgingival calculus by laser-fluorescence in vitro. Lasers Med Sci 2003;18(1):32–35. [PubMed: 12627270]
5. Krause F, Braun A, Jepsen S, Frentzen M. Detection of subgingival calculus with a novel LED-based optical probe. J Periodontol 2005;76(7):1202–1206. [PubMed: 16018765]
6. Kurihara E, Koseki T, Gohara K, Nishihara T, Ansai T, Takehara T. Detection of subgingival calculus and dentine caries by laser fluorescence. J Periodontal Res 2004;39(1):59–65. [PubMed: 14687229]
7. Qin YL, Luan XL, Bi LJ, et al. Real-time detection of dental calculus by blue-LED-induced fluorescence spectroscopy. J Photochem Photobiol B 2007;87(2):88–94. [PubMed: 17433705]
8. Rams TE, Alwaqyan AY. In vitro performance of DIAGNOdent laser fluorescence device for dental calculus detection on human tooth root surfaces. Saudi Dent J 2017;29(4):171–178. [PubMed: 29033528]
9. Shakibaie F, Walsh LJ. Laser fluorescence detection of subgingival calculus using the DIAGNOdent Classic versus periodontal probing. Lasers Med Sci 2016;31(8):1621–1626. [PubMed: 27435218]
10. Tung OH, Lee SY, Lai YL, Chen HF. Characteristics of subgingival calculus detection by multiphoton fluorescence microscopy. J Biomed Opt 2011;16(6):066017. [PubMed: 21721818]
11. Kao MC, Lin CL, Kung CY, Huang YF, Kuo WC. Miniature endoscopic optical coherence tomography for calculus detection. Appl Opt 2015;54(24):7419–7423. [PubMed: 26368780]
12. Tsuda H, Arends J. Raman spectra of human dental calculus. J Dent Res 1993;72(12):1609–1613. [PubMed: 8254131]
13. Tsuda H, Jongebloed WL, Stokroos I, Arends J. A micro-Raman spectroscopic study of hydrazine-treated human dental calculus. Scanning Microsc 1996;10(4):1015–1023. discussion 1023–1014 [PubMed: 9854853]
14. Hsieh YS, Ho YC, Lee SY, et al. Subgingival calculus imaging based on swept-source optical coherence tomography. J Biomed Opt 2011;16(7):071409. [PubMed: 21806255]
15. Huminicki A, Dong C, Cleghorn B, Sowa M, Hewko M, Choo-Smith LP. Determining the effect of calculus, hypocalcification, and stain on using optical coherence tomography and polarized Raman spectroscopy for detecting white spot lesions. Int J Dent 2010;2010:879252–879257. [PubMed: 20652044]
16. Yang VB, Curtis DA, Fried D. Cross-polarization reflectance imaging of root caries and dental calculus at wavelengths from 400-2350-nm. J Biophotonics 2018;11(11):e201800113. [PubMed: 29952066]
17. Jones RS, Huynh GD, Jones GC, Fried D. Near-IR Transillumination at 1310-nm for the Imaging of Early Dental Caries. Opt Express 2003;11(18):2259–2265. [PubMed: 19466117]
18. Buhler C, Ngaotheppitak P, Fried D. Imaging of occlusal dental caries (decay) with near-IR light at 1310-nm. Opt Express 2005;13(2):573–582. [PubMed: 19488387]
19. Staninec M, Lee C, Darling CL, Fried D. In vivo near-IR imaging of approximal dental decay at 1,310 nm. Lasers Surg Med 2010;42(4):292–298. [PubMed: 20432277]
20. Chung S, Fried D, Staninec M, Darling CL. Multispectral near-IR reflectance and transillumination imaging of teeth. Biomed Opt Express 2011;2(10):2804–2814. [PubMed: 22025986]

21. Fried WA, Chan KH, Fried D, Darling CL. High contrast reflectance imaging of simulated lesions on tooth occlusal surfaces at near-IR wavelengths. Lasers Surg Med 2013;45(8):533–541. [PubMed: 23857066]
22. Simon JC, Lucas SA, Lee RC, et al. Near-IR transillumination and reflectance imaging at 1300-nm and 1500–1700-nm for in vivo caries detection. Lasers Surg Med 2016;48(6):828–836. [PubMed: 27389018]
23. Stookey GK. Quantitative light fluorescence: A technology for early monitoring of the caries process. Dent Clin North Am 2005;49(4):753–770. [PubMed: 16150315]
24. Tranaeus S, Al-Khateeb S, Bjorkman S, Twetman S, Angmar-Mansson B. Application of quantitative light-induced fluorescence to monitor incipient lesions in caries-active children. A comparative study of remineralisation by fluoride varnish and professional cleaning. Eur J Oral Sci 2001;109(2):71–75. [PubMed: 11347658]
25. Tranaeus S, Shi XQ, Lindgren LE, Trollsas K, Angmar-Mansson B. In vivo repeatability and reproducibility of the quantitative light-induced fluorescence method. Caries Res 2002;36(1):3–9. [PubMed: 11961323]
26. Alfano RR, Lam W, Zarrabi HJ, Alfano MA, Cordero J, Tata DB. Human teeth with and without caries studied by laser scattering, fluorescence and absorption spectroscopy. IEEE J Quant Electr 1984;20:1512–1515.
27. Angmar-Masson BA, Al-Khateeb S, Tranaeus S. Intraoral use of quantitative light-induced fluorescence detection method. In: Stookey GK editor. Early Detection of Dental Caries 1; Indianapolis, Indiana: Indiana University School of Dentistry, 1996 pp. 39–50.
28. Ferreira Zandona AG, Analoui M, Beiswanger BB, et al. An in vitro comparison between laser fluorescence and visual examination for detection of demineralization in occlusal pits and fissures. Caries Res 1998;32(3):210–218. [PubMed: 9577987]
29. Almaz EC, Simon JC, Fried D, Darling CL Influence of stains on lesion contrast in the pits and fissures of tooth occlusal surfaces from 800-1600-nm. In: Lasers in Dentistry XXII, Proc. SPIE. Bellingham, WA: SPIE: Vol. 9692. 2016. pp X1–X6.
30. Kleter GA. Discoloration of dental carious lesions (a review). Arch Oral Bio 1998;43:629–632. [PubMed: 9758045]
31. Sarna T, Sealy RC. Photoinduced oxygen consumption in melanin systems. Action spectra and quantum yields for eumelanin and synthetic melanin. Photochem Photobiol 1984;39:69–74. [PubMed: 6422483]
32. Fu D, Ye T, Matthews TE, Yurtsever G, Warren WS. Two-color, two-photon, and excited-state absorption microscopy. J Biomed Opt 2007;12(5):054004. [PubMed: 17994892]
33. Aoki A, Ando Y, Watanabe H, Ishikawa I. In vitro studies on laser scaling of subgingival calculus with an erbium:YAG laser. J Periodontol 1994;65(12):1097–1106. [PubMed: 7877081]
34. Aoki A, Miura M, Akiyama F, et al. In vitro evaluation of Er:YAG laser scaling of subgingival calculus in comparison with ultrasonic scaling. J Periodontal Res 2000;35(5):266–277. [PubMed: 11005154]
35. Radvar M, Creanor SL, Gilmour WH, et al. An evaluation of the effects of an Nd:YAG laser on subgingival calculus, dentine and cementum. An in vitro study. J Clin Periodontol 1995;22(1):71–77. [PubMed: 7706542]
36. Rechmann P Dental laser research: Selective ablation of caries, calculus, and microbial plaque: From the idea to the first in vivo investigation. Dent Clin North Am 2004;48(4):1077–1104. [PubMed: 15464565]
37. Ting CC, Fukuda M, Watanabe T, Aoki T, Sanaoka A, Noguchi T. Effects of Er,Cr:YSGG laser irradiation on the root surface: Morphologic analysis and efficiency of calculus removal. J Periodontol 2007;78(11):2156–2164. [PubMed: 17970683]
38. Tucker D, Cobb CM, Rapley JW, Killoy WJ. Morphologic changes following in vitro CO2 laser treatment of calculus-ladened root surfaces. Lasers Surg Med 1996;18(2):150–156. [PubMed: 8833283]
39. Yan R, Chan KH, Tom H, Simon JC, Darling CL, Fried D Selective removal of dental caries with a diode-pumped Er:YAG laser. In: Lasers in Dentistry XX, Proc. SPIE. Bellingham, WA: SPIE: Vol. 9306. 2015. pp O1–O8.

40. Stock K, Diebolder R, Hausladen F, Hibst R Efficient bone cutting with the novel diode pumped Er:YAG laser system: In vitro investigation and optimization of the treatment parameters. In: Photonic Therapeutics and Diagnostics X, Proc. SPIE. Bellingham, WA: SPIE: Vol. 8926. 2014. pp P1–P6.
41. Stock K, Diebolder R, Hausladen F, Wurm H, Lorenz S, Hibst R Primary investigations on the potential of a novel diode pumped Er:YAG laser system for bone surgery. In: Photonic Therapeutics and Diagnostics IX, Proc. SPIE. Bellingham, WA: SPIE: Vol. 8565. 2013. pp D1–D8.
42. Stock K, Hausladen F, Hibst R Investigations on the potential of a novel diode pumped Er:YAG laser system for dental applications. In: Lasers in Dentistry XVIII, Proc. SPIE. Bellingham, WA: SPIE: Vol. 8208. 2012. pp D1–D5.
43. Fried WA, Chan KH, Darling CL, Fried D. Use of a DPSS Er:YAG laser for the selective removal of composite from tooth surfaces. Biomed Opt Express 2016;9(10):5026–5036.
44. Myers TD, Myers WD. The use of a laser for debridement of incipient caries. J Prosthet Dent 1985;53:776–779. [PubMed: 3859646]
45. Harris DM, White JM, Goodis H, et al. Selective ablation of surface enamel caries with a pulsed Nd:YAG dental laser. Lasers Surg Med 2002;30(5):342–350. [PubMed: 12116326]
46. Hibst R, Keller U. Experimental studies of the application of the Er:YAG laser on dental hard substances: I. Measurement of the ablation rate. Lasers Surg Med 1989;9:338–344. [PubMed: 2761329]
47. Hennig T, Rechmann P, Jeitner P Effects of a second harmonic Alexandrite laser on human dentin. In: Advanced Laser Dentistry, Proc. SPIE. Bellingham, WA: SPIE: Vol. 1984. 1995. pp 24–30.
48. Hennig T, Rechmann P, Jeitner P, Kaufmann R Caries-selective ablation: The second threshold. In: Lasers in Orthopedic, Dental, and Veterinary Medicine II, Proc. SPIE. Bellingham, WA: SPIE: Vol. 1880. 1993. pp 117–123.
49. Hennig T, Rechmann P, Pilgrim C, Kaufmann R. Basic principles of caries selective ablation by pulsed lasers. In: Proceedings of the Third International Congress on Lasers in Dentistry. 1992. pp 119–120.
50. Hennig T, Rechmann P, Pilgrim CG, Schwarzmaier H-J, Kaufmann R Caries selective ablation by pulsed lasers. In: Lasers in Orthopedic, Dental, and Veterinary Medicine, Proc. SPIE. Bellingham, WA: SPIE: Vol. 1424. 1991. pp 99–104.
51. Fan K, Fried D Scanning ablation of root caries with acoustic feedback control. In: Lasers in Dentistry XIII, Proc. SPIE. Bellingham, WA: SPIE: Vol. 6425. 2007. pp J1–J7.
52. Arima MK, Matsumoto K. Effects of aRF: Excimer laser irradiation on human enamel and dentin. Lasers Surg Med 1993;13:97–105. [PubMed: 8426533]
53. Schoenly JE, Seka W, Rechmann P. Pulsed laser ablation of dental calculus in the near ultraviolet. J Biomed Opt 2014;19(2):028003. [PubMed: 24549442]
54. Schoenly JE, Seka WD, Rechmann P. Near-ultraviolet removal rates for subgingival dental calculus at different irradiation angles. J Biomed Opt 2011;16(7):071404. [PubMed: 21806250]
55. Eberhard J, Bode K, Hedderich J, Jepsen S. Cavity size difference after caries removal by a fluorescence-controlled Er:YAG laser and by conventional bur treatment. Clin Oral Investig 2008;12(4):311–318.
56. Eberhard J, Eisenbeiss AK, Braun A, Hedderich J, Jepsen S. Evaluation of selective caries removal by a fluorescence feedback-controlled Er:YAG laser in vitro. Caries Res 2005;39(6):496–504. [PubMed: 16251795]
57. Jepsen S, Acil Y, Peschel T, Kargas K, Eberhard J. Biochemical and morphological analysis of dentin following selective caries removal with a fluorescence-controlled Er:YAG laser. Lasers Surg Med 2008;40(5):350–357. [PubMed: 18563782]
58. Tao YC, Fried D. Near-infrared image-guided laser ablation of dental decay. J Biomed Opt 2009;14(5):054045. [PubMed: 19895146]
59. Krause F, Braun A, Brede O, Eberhard J, Frentzen M, Jepsen S. Evaluation of selective calculus removal by a fluorescence feedback-controlled Er:YAG laser in vitro. J Clin Periodontol 2007;34(1):66–71. [PubMed: 17132156]

60. Chan KH, Tom H, Darling CL, Fried D Serial removal of caries lesions from tooth occlusal surfaces using near-IR image-guided IR laser ablation. In: Lasers in Dentistry XIX, Proc. SPIE. Bellingham, WA: SPIE: Vol. 9306. 2015. pp M1–M7.

61. Chan KH, Fried D. Selective ablation of dental caries using coaxial CO2 (9.3-μm) and near-IR (1880-nm) lasers. Lasers Surg Med 2019;51:176–184. [PubMed: 30024032]

62. Tom H, Chan KH, Darling CL, Pelzner R, Fried D. Selective removal of demineralized enamel using a CO laser coupled with near-IR reflectance imaging. Lasers Surg Med 2016;48(1):52–61. [PubMed: 26763111]

63. Chan KH, Hirasuna K, Fried D. Rapid and Selective Removal of Composite from Tooth Surfaces with a 9.3-μm CO2 Laser using Spectral Feedback. Lasers Surg Med 2011;43(8):824–832. [PubMed: 21956630]

64. Chan KH, Hirasuna K, Fried D. Analysis of enamel surface damage after selective laser ablation of composite from tooth surfaces. Photonics Lasers Med 2014;3(1):37–45. [PubMed: 24707453]

65. Jang AT, Chan KH, Fried D. Automated ablation of dental composite using an IR pulsed laser coupled to a plume emission spectral feedback system. Lasers Surg Med 2017;49(7):658–665. [PubMed: 28467687]

66. Bush J, Feldchtein F, Gelikonov G, Gelikonov V, Piyevsky S Cost effective all-fiber autocorrelator for optical coherence tomography imaging. In: 17th International Conference on Optical Fibre Sensors, Proc. SPIE. Bellingham, WA: SPIE: Vol. 5855. 2005. pp 254–257.

67. Bozbay E, Dominici F, Gokbuget AY, et al. Preservation of root cementum: A comparative evaluation of power-driven versus hand instruments. Int J Dent Hyg 2018;16(2):202–209. [PubMed: 27860247]

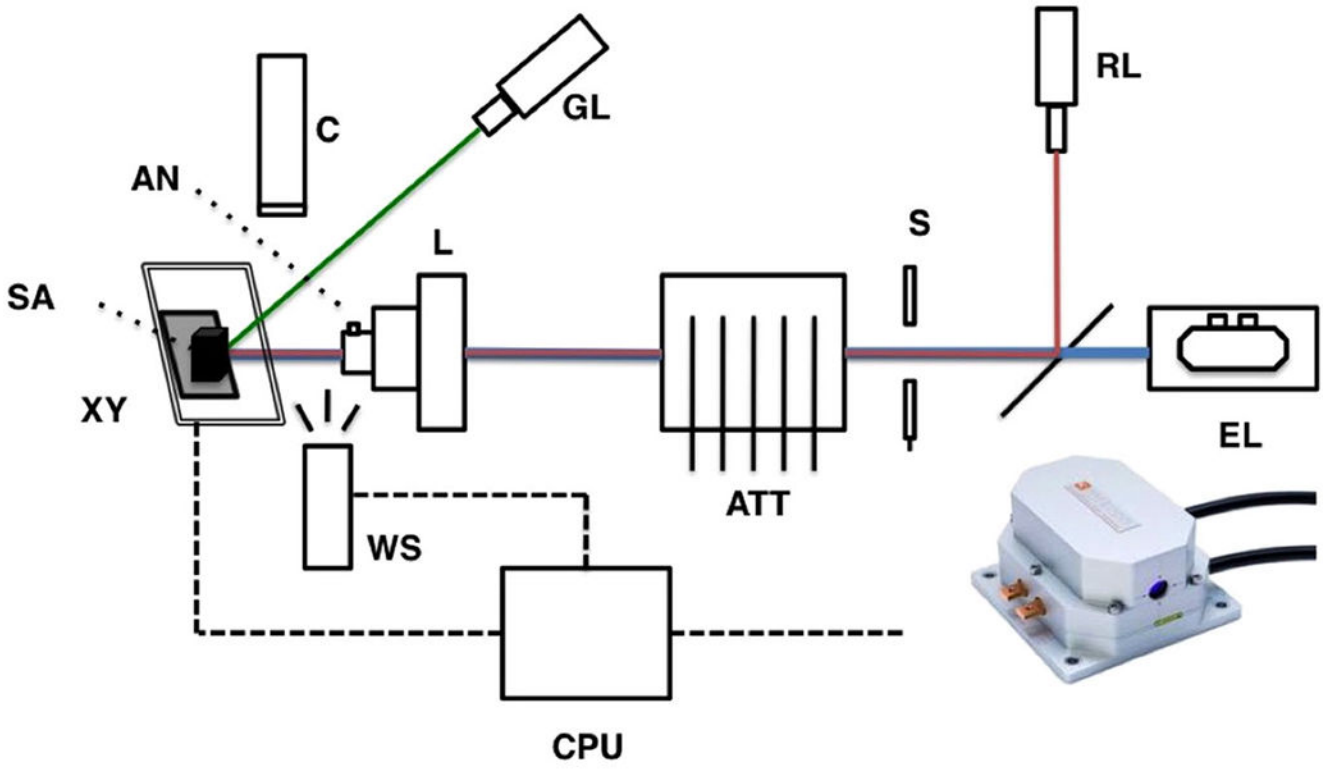

Fig. 1.

Laser setup with DPSS Er:YAG laser (EL), green and red targeting lasers (GL & RL), shutter (S), glass slide attenuators (ATT), lens (L), XY stage (XY), sample (SA), air nozzle (AN), camera (C), water spray (WS), and computer (CPU). An image of the DPSS Er:YAG laser is shown on lower right.

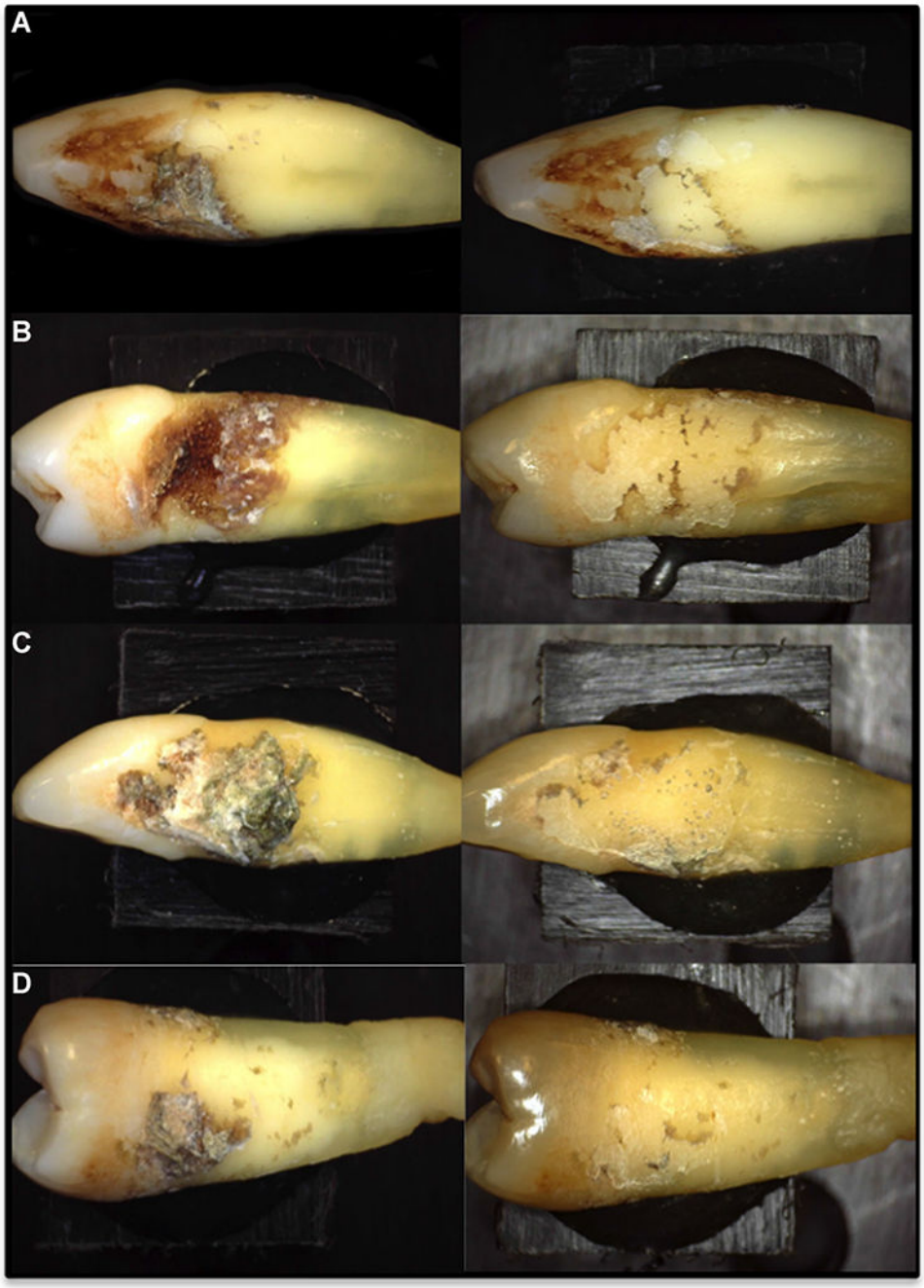

Fig. 2.

Color images of four different samples (**A**–**D**) before (left) and after (right) laser removal of the exposed calculus deposits residing on the root surface.

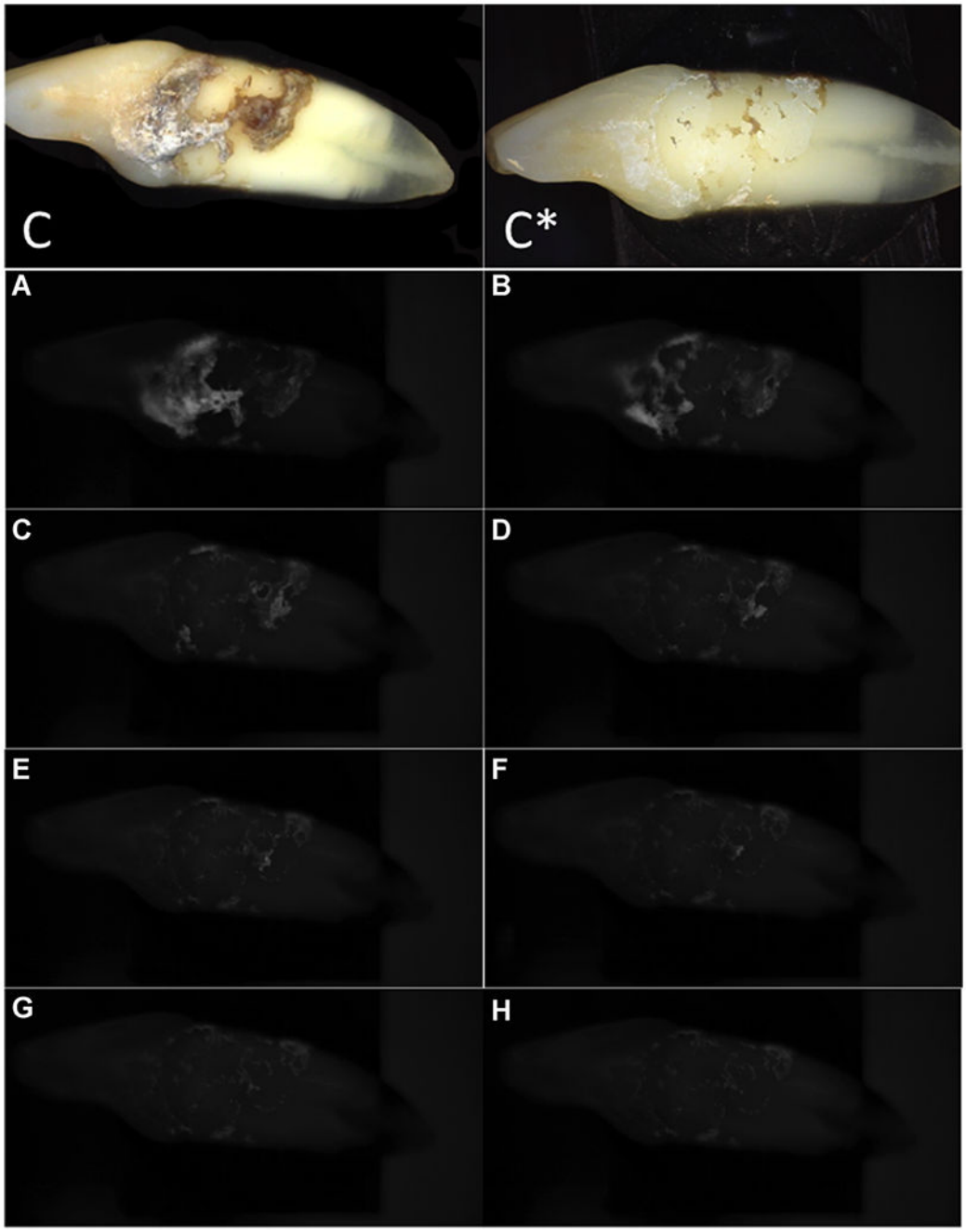

Fig. 3.

Color images (**C** and **C***) before and after calculus removal along with sequential near-infrared reflectance images taken between each laser ablation scan (**A**–**H**) for one of the samples.

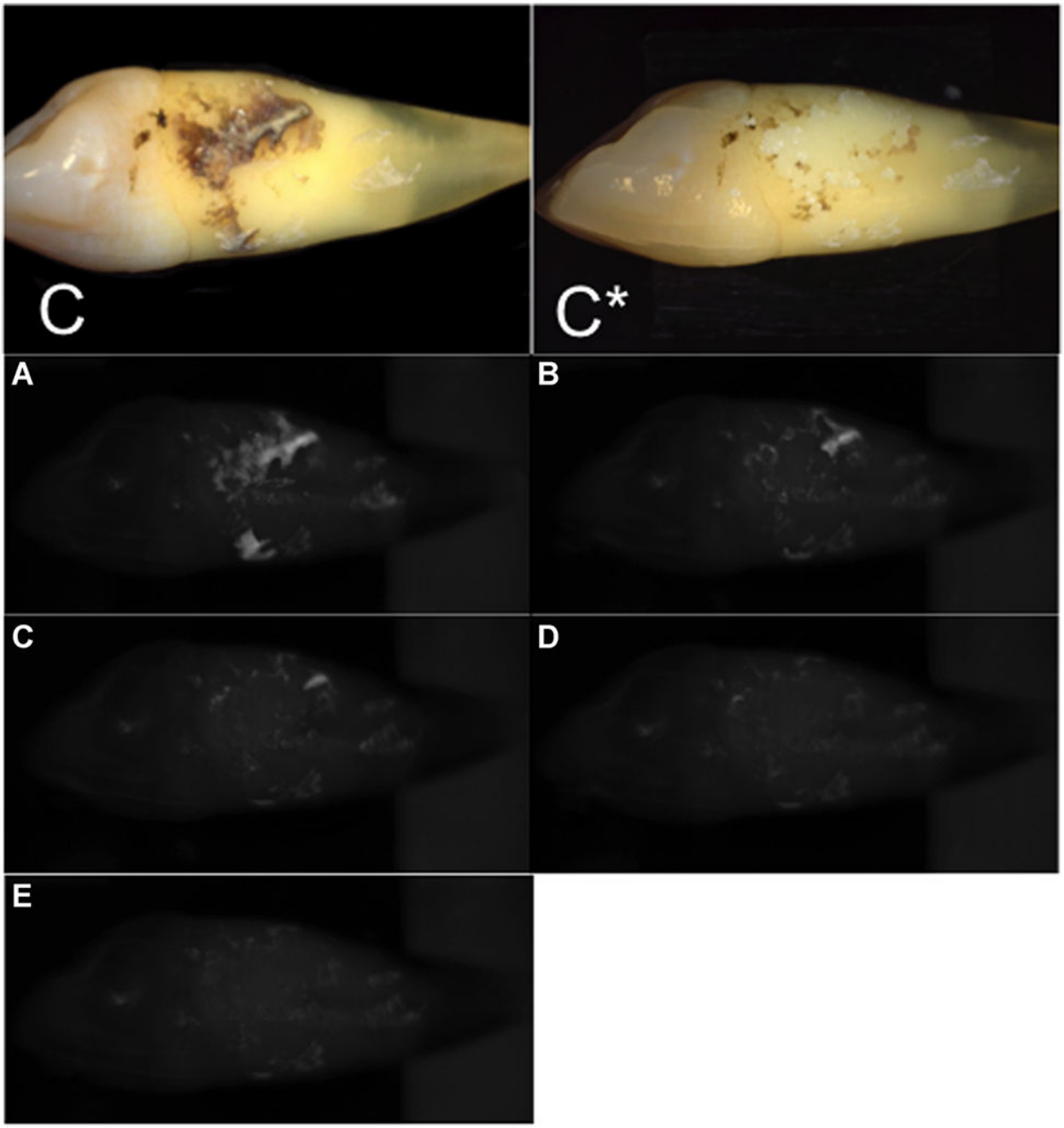

Fig. 4.

Color images (**C** and **C***) before and after calculus removal along with sequential near-infrared reflectance images taken between each laser ablation scan (**A**–**E**) for one of the samples.

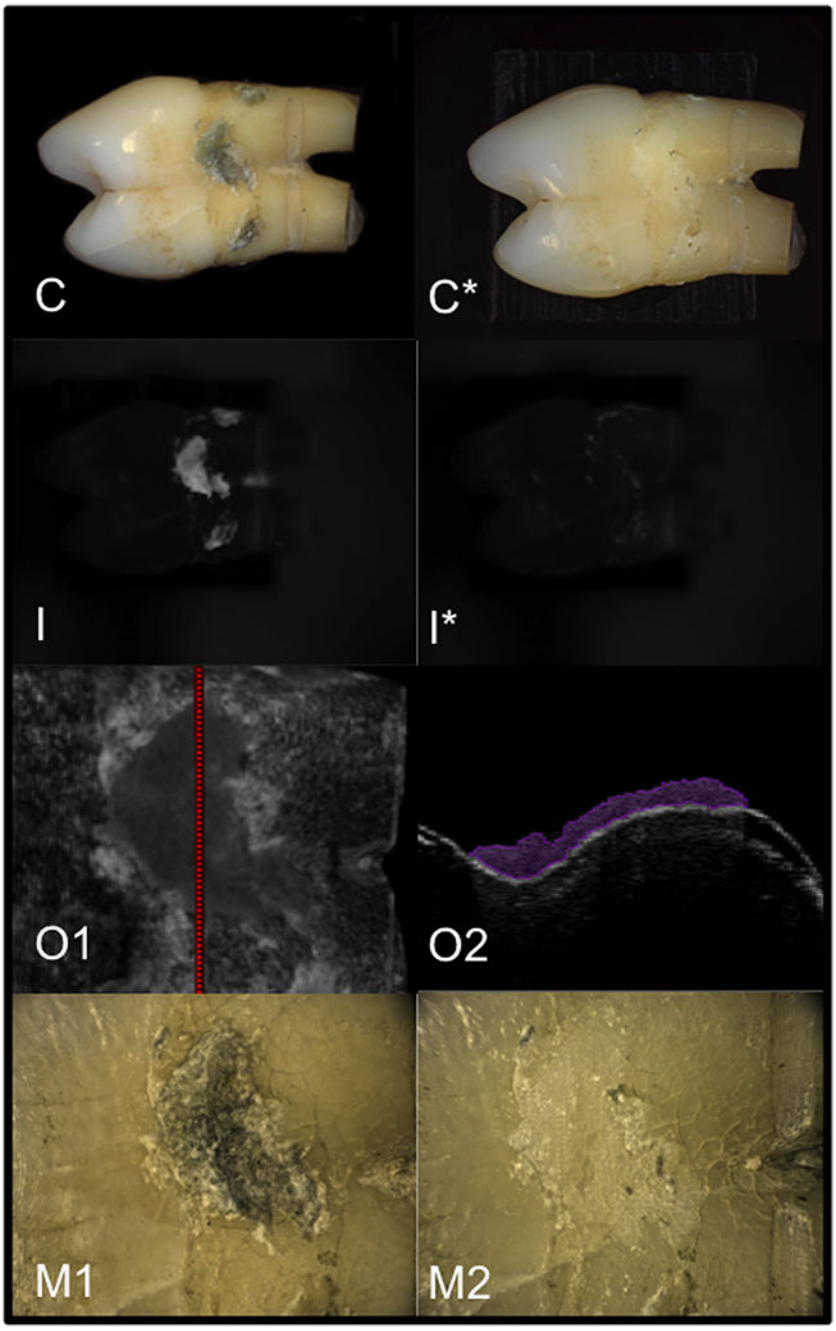

Fig. 5.

Color images (**C** and **C***) and near infrared (**I** and **I***) before and after calculus removal. (**O1**) A surface rendering of the three-dimensional optical coherence tomography (OCT) image is shown with the position of the extracted b-scan (**O2**) indicated by the red line. Overlays of co-registered OCT scans were used to determine the calculus removed shown in purple and the damage to the underlying cementum shown in green. Digital microscopy images taken at ×50 magnification show the laser-irradiated area pre- (**M**) and post-treatment (**M***).

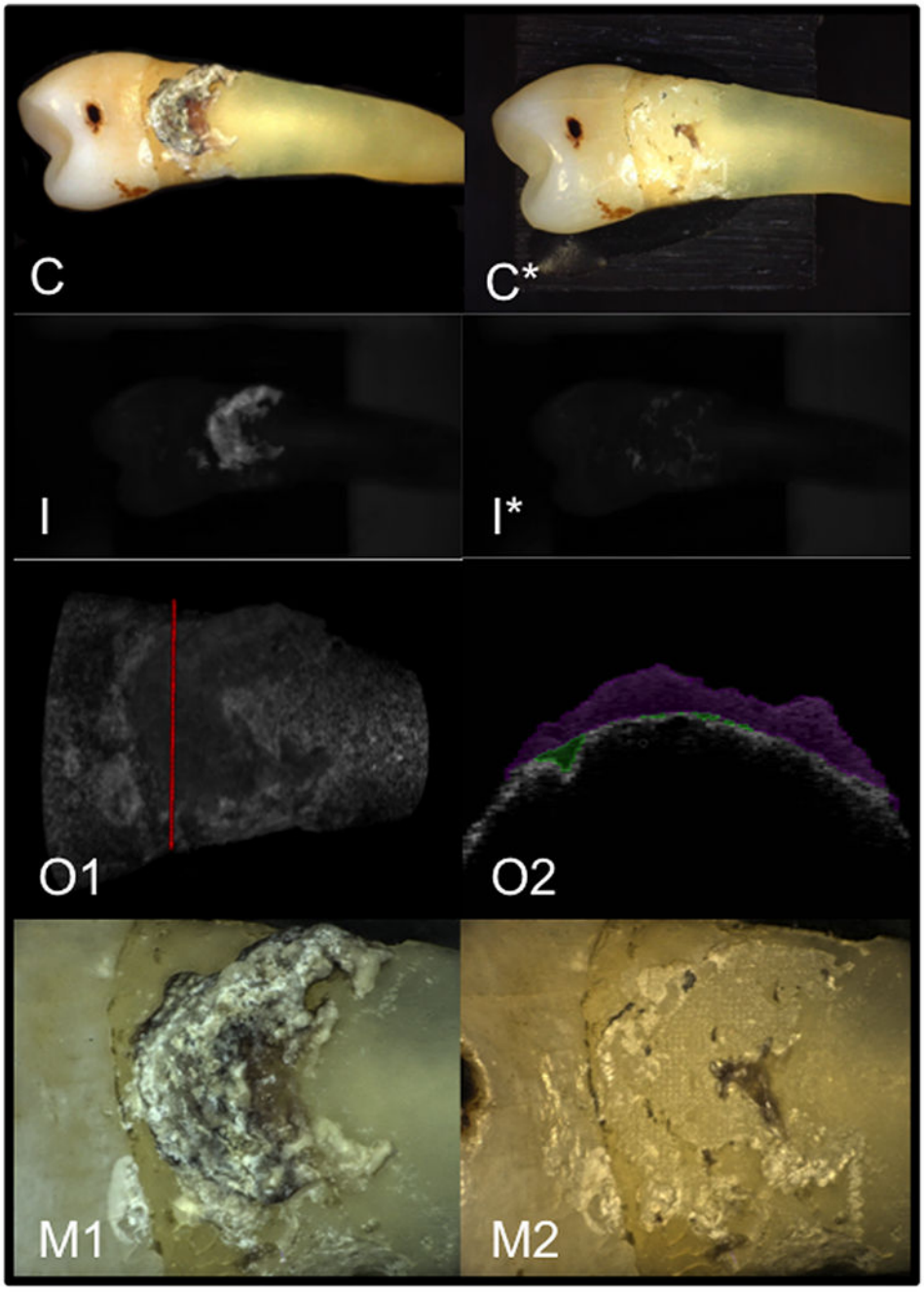

Fig. 6.

Color images (**C** and **C***) and near infrared (**I** and **I***) before and after calculus removal. (**O1**) A surface rendering of the three-dimensional optical coherence tomography (OCT) image is shown with the position of the extracted b-scan (**O2**) indicated by the red line. Overlays of co-registered OCT scans were used to determine the calculus removed shown in purple and the damage to the underlying cementum shown in green. Digital microscopy images taken at ×50 magnification show the laser-irradiated area pre- (**M**) and post-treatment (**M***).

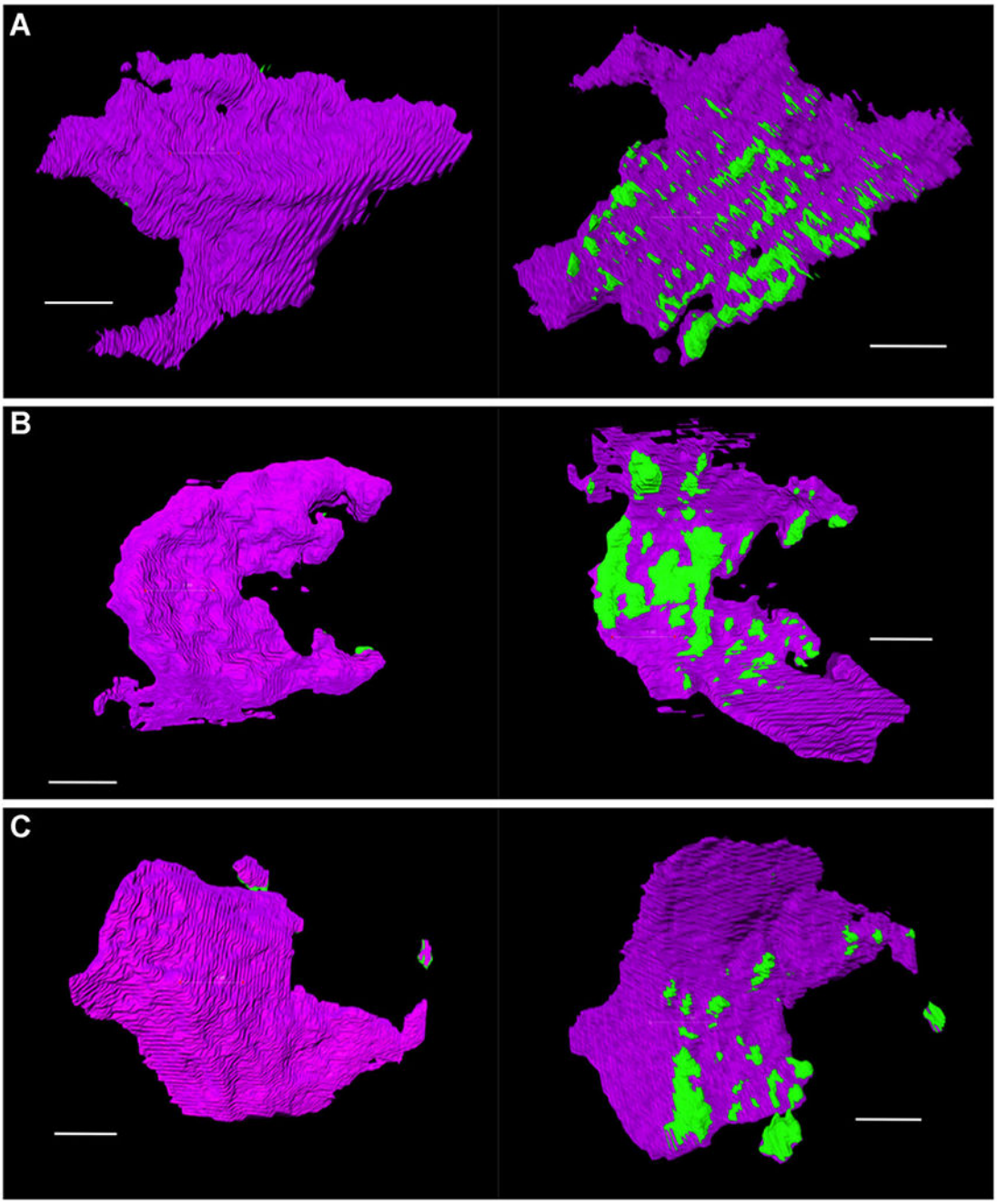

Fig. 7.

Three-dimensional surface renderings of the volumes of calculus (purple) and cementum lost (green) are shown for three of the teeth. The top (left) and bottom (right) views are shown for the body of calculus for each tooth. The bottom view is a mirror image of the top view, i.e. to compare positions on the two images the bottom image needs to be flipped vertically. The body of calculus in (**A**) is from the tooth shown in Figure 2A, (**B**) is from the tooth shown in Figure 6, and (**C**) is from the tooth shown in Figure 2D. The position of the

cementum enamel junction relative to each body of calculus is the center of the figure, that is to the right of the top view of the calculus and to the left of the bottom view.

TABLE 1.

Calculus and Cementum Measurements for Each of the 10 Samples

Tooth	Mean Calculus Thickness (mm)	Max Depth Cementum Damage (mm)	Max Residual Calculus Height (mm)	Mean Calculus Removed Per Slice (mm^3)	Mean Cementum Removed Per Slice (mm^3)
1	0.56	0.13	0.26	0.042	0.0014
2	0.92	0.33	0.30	0.069	0.0013
3	0.61	0.19	0.31	0.055	0.00058
4	0.54	0.40	0.17	0.029	0.0044
5	0.52	0.25	0.12	0.040	0.0044
6	0.39	0.17	0.24	0.032	0.0015
7	0.35	0.19	0.24	0.024	0.00063
8	0.33	0.25	0.18	0.026	0.00074
9	0.84	0.11	0.58	0.1	0.00072
10	0.37	0.10	0.22	0.016	0.00024

The values in the last two columns represent the mean calculus and cementum removed for the five slices that were analyzed from each sample.